# Complexity of modulation instability

Auro M. Perego[*,†] and Florent Bessin[†]

*Aston Institute of Photonic Technologies, Aston University, Birmingham B4 7ET, United Kingdom*

Arnaud Mussot

*University of Lille, CNRS, UMR 8523-PhLAM-Physique des Lasers Atomes et Molécules, F-59000 Lille, France*

In this Research Letter, using experimental data, we analyze the computational complexity of modulation instability of a light wave propagating in a single-mode optical fiber. We show that computational complexity is an excellent tool which provides an insight into the emergence from noise of modulation-instability-induced coherent structures in the linear stage, before they become fully developed in the temporal traces, and substantially anticipating other statistical methods. Furthermore, computational complexity captures qualitatively the statistical signature of the recurrences in the nonlinear stage of modulation instability too.

The nonlinear Schrödinger equation (NLSE) is a paradigmatic universal model which describes nonlinear dispersive waves across the most diverse areas of physics including fluid dynamics [1], plasmas [2], Bose-Einstein condensates, and nonlinear optics [3]. One of the most significant and studied phenomena described by the NLSE is definitely the modulation instability (MI) of its homogeneous solution [4]. MI occurs when a weak periodic perturbation grows exponentially at the expense of a strong carrier wave. This phenomenon results in the generation of temporal periodic patterns and in the birth of spectral symmetrical sidebands on both sides of the carrier wave frequency that eventually result in the breakup of the original wave itself. It has been observed in a variety of physical systems including fluids, plasmas, Bose-Einstein condensates, and fiber optics. In nonlinear fiber optics the first experimental observation of MI dates back to 1986 [5]. While MI has been firstly evidenced in the spectral domain, the direct observation of the associated temporal dynamics has remained for a long time a considerable challenge due to the very fast nature of its oscillations, which in general exceed the bandwidth of electronic devices. Impressive recent advancements in measurement techniques such as time lenses, time microscopy, and time holography [6–8] have finally enabled the observation of the complex temporal dynamics of MI. These recent observations contributed to get a deeper understanding of the MI phenomena.

The linear stage of MI is characterized by exponential growth of spectral sidebands which can be mathematically described by two linearized coupled differential equations for the perturbations amplitudes. However, when modulation mode amplitudes become significant compared with the central mode, nonlinear terms in the perturbation equations become relevant: The linearization approximation breaks down, and a rich and complex dynamics appears. The most striking feature of the nonlinear stage of MI lies with recurrences associated with the Fermi-Pasta-Ulam-Tsingou (FPUT) problem. This is linked to the energy oscillating back and forth between the sidebands and the homogeneous mode [9–12]. In the time domain, soliton- and breather-like coherent structures appear and dynamically interact. Due to the complexity of the nonlinear stage of MI, advanced characterization tools such as the autocorrelation function [13–15], the probability distribution function of the intensity [14,16], and sophisticated concepts such as the soliton gas theory [17] are required to capture and describe its complex dynamics. However, the abovementioned statistical tools do not provide information about the self-organization process when the embryonic coherent structures are embedded in noise and cannot yet be macroscopically detected in the temporal traces. MI is an intrinsically complex phenomenon where a nontrivial interplay between noise and nonlinearity shapes the dynamics [18]. Providing a quantitative measure of complexity in a variety of systems is a relevant research topic in physics where different approaches have been explored in many different contexts [19]. For instance, in recent years, complexity in various nonlinear photonic systems has been investigated [20–23], exploiting the framework of the spin glass theory [24,25].

In different fields of nonlinear science it has been shown that *computational complexity* can provide relevant information about the pattern formation process [26]. To the best of our knowledge, the computational complexity of temporal intensity traces generated by MI has never been investigated or computed so far. Shedding light on the relevance of this statistical quantity for the understanding and prediction of MI in optical fibers is the main goal of this Research Letter. Here

---

[*]a.perego1@aston.ac.uk
[†]These authors contributed equally to this work.

we will focus specifically on the concept of computational complexity of a string which was introduced by Kolmogorov in 1963 [27]. Within this theoretical framework, the computational complexity of one string is the length (in bits) of the shortest computer program that is able to produce that particular string as an output. A universal way to calculate the computational complexity of a string is not available. However, one of the possible methods to calculate it for a binary string is based on the Lempel-Ziv (LZ) algorithm [28]. The latter constitutes the foundation of various file compression protocols currently used in personal computers. The LZ algorithm assumes that the program, which has to compute a given string, can only do two operations: copy a substring or insert a new substring. We summarize here very briefly the LZ algorithm following Ref. [26], where an excellent diagrammatic representation can be found too. Let us consider a string $\sigma$ made of digits $\sigma_1\sigma_2\cdots\sigma_n$ that has been reconstructed up to digit $\sigma_r$, and let us call $\Sigma = \sigma_1\sigma_2\cdots\sigma_r$ the reconstructed part of the string. We now consider a substring of $\sigma$, $Q = \sigma_{r+1}$, and check whether $Q$ can be reconstructed by simply copying substrings of $\Sigma$: If yes, we define a new $Q = \sigma_{r+1}\sigma_{r+2}$, and so on and so forth till $Q$ cannot be reconstructed anymore copying words from substrings of $\Sigma$. In this case a new digit has to be inserted to create $Q$. The total number of inserted digits (plus 1 if the last copy step is not followed by adding a digit) is defined as the computational complexity $c(n)$ of the string, and it basically consists in the total number of steps necessary to construct the full string $\sigma$. However, a more convenient indicator is the complexity normalized as $C(n) = c(n)/b(n)$, where $b(n) = \lim_{n\to\infty} c(n) = \frac{n}{\log_2(n)}$ is the asymptotic value of the $c(n)$ for a randomly ordered binary string [26,28]. Hence, for $n \to \infty$, $C(n)$ will tend to 1 for a string where 0s and 1s are randomly ordered and will be close to 0 for a string whose digits are arranged in a periodic pattern (e.g., $010101\cdots$) or are all perfectly identical to 0, or to 1.

It is crucial to mention that computational complexity differs substantially from the Shannon entropy (SE), a cornerstone of information theory introduced by Shannon in 1948 [29]. A binary string consisting of $n$ digits, of which $n_0$ is the number of 0s and $n_1$ is the number of 1s, has SE given by $S = -\sum_{m=0}^{1} p_m \log_2(p_m)$, where $p_{0,1} = n_{0,1}/n$. SE has a maximum for a string where $p_1 = p_0 = 1/2$. On the other hand, it tends to zero for either ($p_1 \to 1$, $p_0 \to 0$) or ($p_1 \to 0$, $p_0 \to 1$). Hence SE is a measure of the randomness, or indeed entropy, of the source that produces the string. However, SE does not provide any knowledge regarding the sequential order in which the 0s and 1s are arranged within the string. Things are very different for the computational complexity. For instance, a string with 0s and 1s alternating periodically ($01010\cdots$) has normalized computational complexity close to 0, according to the LZ algorithm, which is very different from the normalized computational complexity of a string having the same number of 0s and 1s but arranged in completely random fashion, which has normalized computational complexity close to 1. In contrast, SE would be the same for both strings. Thus computational complexity can be used to provide knowledge about the structure and order of the data that is not captured by SE. When $C(n)$ is significantly smaller than 1, then we have a clear indication of the existence of regular patterns or coherent structures in
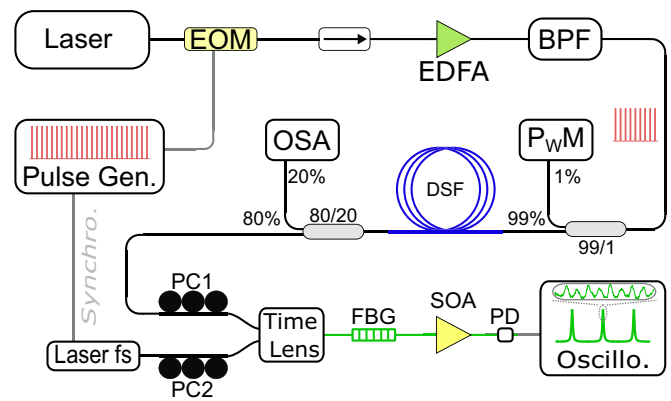


FIG. 1. Experimental setup: EOM, electro-optic modulator; EDFA, erbium-doped fiber amplifier; BPF, bandpass filter; $P_W$M, power meter; DSF, dispersion-shifted fiber; OSA, optical spectrum analyzer; PC$_{1-2}$, polarization controller; Laser fs, femtosecond laser; FBG, fiber Bragg grating; SOA, semiconductor optical amplifier; PD, photodetector; Oscillo., oscilloscope; Pulse Gen., pulse generator; Synchro., synchronization.

the data. Incidentally, we note that an analysis based on SE of spatial MI of light in nonlocal media has been presented in Ref. [30]. It is important to mention that computational complexity is an extremely powerful metric tool to characterize, for instance, not only temporal traces generated in various systems especially in biology including electroencephalogram [31,32], electrocardiogram [33], and neural spike [34] traces, but also the structure of DNA sequences [35]. Furthermore, computational complexity has been used to analyze patterns and chaos in dynamical systems including coupled logistic maps and cellular automata [26] also in comparison with other mathematical tools such as Lyapunov exponents. One key finding of Ref. [26] is that computational complexity can reveal pattern formation before its appearance is manifest in the autocorrelation function or macroscopically in the amplitude traces. To test the ability of computational complexity to characterize MI of light, we have experimentally generated a series of binary strings through the MI process of continuous wave (cw) radiation propagating inside a single-mode optical fiber. Then, we computed the evolution of their computational complexity as a function of the input power $P_{in}$ because the number of nonlinear lengths, $L_{NL}$, scales as $1/P_{in}$ [36] and rules the change in system complexity.

We provide a detailed schematic of the experimental setup in Fig. 1. We have used as a light source a cw laser emitting at 1545 nm wavelength. Light intensity was chopped by means of an electro-optic modulator driven by an arbitrary wave generator to produce square-shaped pulses with a duration of 1 ns. Then, these pulses were amplified by an erbium-doped fiber amplifier whose amplified spontaneous emission in excess was removed by a thin bandpass filter (100 GHz bandwidth). Next, amplified pulses were launched in a 4.186-km-long specially designed dispersion-shifted fiber (DSF), with group velocity $\beta_2 = -4.4$ ps$^2$ km$^{-1}$, nonlinearity $\gamma = 2.5$ W$^{-1}$ km$^{-1}$, and losses $\alpha = 0.0495$ km$^{-1}$ at 1545 nm. Note that we added a 1% calibrated tap coupler before the DSF in order to measure with a power meter the launched power. By using a 80/20 coupler, we were able to study the

DSF output signal by means of an optical spectral analyzer (OSA) and a commercial time lens (PicoLuz ultrafast temporal magnifier; Thorlabs) based on the results published in Ref. [37]. The time-stretching effect provided by the time lens was obtained thanks to a four-wave-mixing (FWM) process between a strong pump and the fiber output signal to analyze. The strong pump was generated by a femtosecond laser centered at 1570 nm with a fixed repetition rate of 99.882 MHz. This laser was also used as a reference clock for the electro-optic modulator; in that way, the repetition rate of the pump pulses was a multiple of the femtosecond laser (10 times in our case). This ensured a perfect overlap between femtosecond pump pulses and DSF output pulses. Note that we added polarization controllers before the time lens (PC$_{1-2}$) in order to optimize the FWM process efficiency. The magnified signal (idler generated from the FWM process, magnification factor of 57) was isolated from the rest of the components by a fiber Bragg grating (FBG). Finally, a semiconductor optical amplifier (SOA) was used to slightly amplify this signal, which was then recorded by a fast photodiode and a broadband oscilloscope (70 GHz bandwidth each). Through this time lens, we were able to record temporal traces of each DSF output pulse over a window and a resolution of about 50 ps and 300 fs, respectively. The recorded temporal traces of the light power were transformed into a binary string $s(t)$ according to the following rule: If $P(t) > \bar{P}$, then $s(t) = 1$, else $s(t) = 0$, with $\bar{P}$ being the average power of the trace. For each value of $P_{in}$, we calculated the computational complexity corresponding to 3994 pulses, and from this set of measurements we computed the averaged normalized computational complexity and the associated standard deviation. We repeated the procedure for 155 different values of the input power $P_{in}$ in the interval [0.3, 4] W. This corresponds to an investigation of the complexity ranging from 3 to 30 $L_{NL}$. We have also simulated numerically the light propagation along the optical fiber by solving the following NLSE for the field envelope $A(z, t)$ defined in a comoving temporal reference frame of coordinate $t$ and evolving along spatial coordinate $z$:

$$\frac{\partial A}{\partial z} = -i\frac{\beta_2}{2}\frac{\partial^2 A}{\partial t^2} + i\gamma |A|^2 A - \frac{\alpha}{2}A. \quad (1)$$

The initial conditions was chosen to be $A(0, t) = \sqrt{P_{in}} + n_a(r_r(t) + ir_i(t))/\sqrt{2}$, where $n_a = 10^{-6}$ W$^{\frac{1}{2}}$ is the noise amplitude and $r_r(t)$ and $r_i(t)$ are random numbers generated independently and uniformly distributed in the interval [0,1]. In simulations we have varied $P_{in}$ in the same interval as in experiments using 185 points. For each value of $P_{in}$ we have repeated the simulation 80 times and obtained the averaged normalized computational complexity $\langle C \rangle$ and average indicators that will be presented below as well. We have furthermore performed an additional set of numerical simulations using a pulsed-envelope initial condition in order to mimic more closely the experimental scenario. In the latter case the initial conditions used are $A_p(0, t) = \sqrt{P_{in}}e^{-\frac{t^6}{\sigma^6}} + n_a(r_r(t) + ir_i(t))/\sqrt{2}$ with $\sigma = 0.38$ ns.

In Fig. 2(a) we have plotted the MI output spectrum versus $P_{in}$ from experiments. Figures 2(b)–2(e) show the output spectra corresponding to different pump powers. Examples of their corresponding time traces are depicted in Figs. 2(f)–2(i).
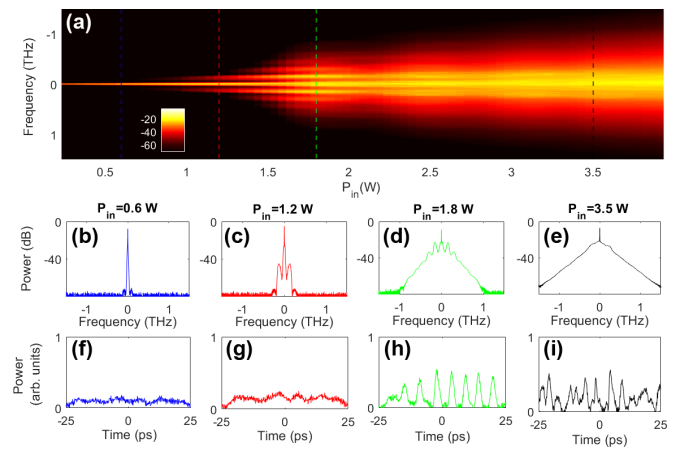


FIG. 2. (a) Evolution of the experimentally measured power spectrum in decibels vs input power $P_{in}$. (b)–(e) Output spectra corresponding to different input power [indicated above each panel and corresponding to the colored dashed lines in (a)]. (f)–(i) Examples of corresponding temporal traces.

The latter exhibit coherent structures embedded in noise in the linear stage, regular coherent structures, and turbulent coherent structures, respectively.

In Fig. 3 we have plotted the evolution of the power trace measured at the fiber output both in experiment and in numerical simulations. For $P_{in}$ between 1.5 and 2 W, we observe the macroscopic manifestation of coherent structures. The main results of this work are summarized in Fig. 4, where we compare the computational complexity obtained from experimental and numerical data with other relevant statistical indicators. In particular, we have considered the following: the second-order moment of the autocorrelation function $\kappa_4$, defined as the autocorrelation function $g^{(2)}(\tau) = \langle P(t + \tau)P(t) \rangle / \langle P(t) \rangle^2$ evaluated at $\tau = 0$ [14]; the previously defined Shannon entropy, and the Shannon spectral entropy (SSE), which measures spectral broadening and is defined as $\hat{S} = -\sum_\omega p_\omega \ln(p_\omega)$, where $p_\omega$ is the amount of power contained in the spectral mode with frequency $\omega$, normalized by the total power in the spectrum. We observe that the computational complexity [Figs. 4(a) and 4(b)]
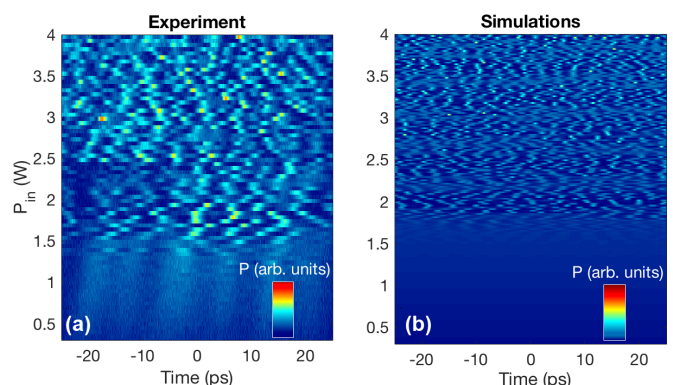


FIG. 3. Pseudospatiotemporal map showing temporal traces at the fiber output plotted in the plane $t$-$P_{in}$: (a) experiment; (b) numerical simulations, for cw input.
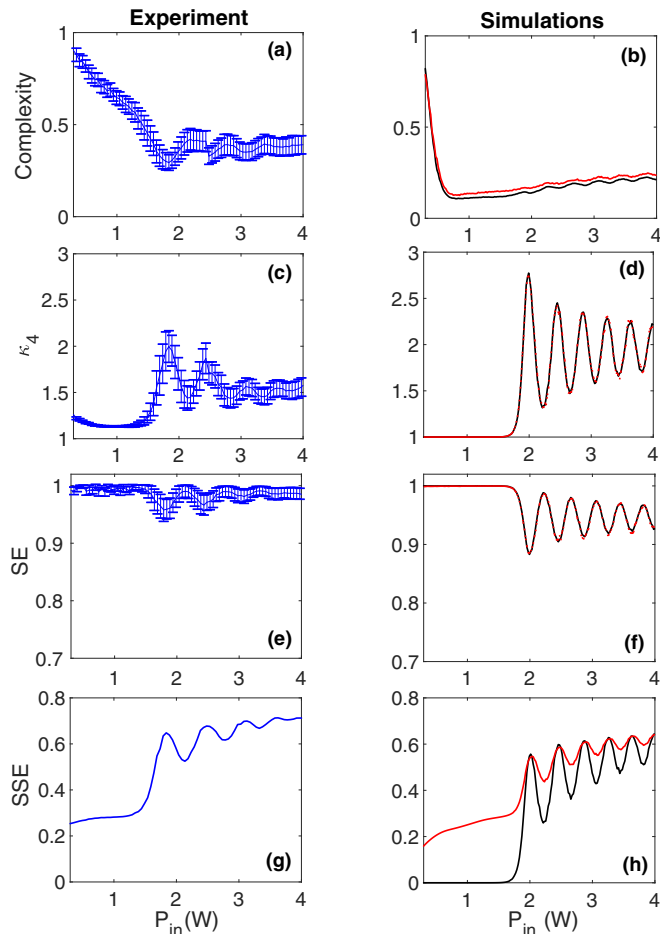
FIG. 4. Complexity $\langle C \rangle$ [(a) and (b)], $\kappa_4$ [(c) and (d)], spectral entropy [(e) and (f)], and spectral Shannon entropy [(g) and (h)] are plotted vs pump power $P_{in}$. Experimental results are shown in the left column, and simulation results are shown in the right column (black lines and red lines correspond to cw and pulsed input, respectively).

TABLE I. Summary of the MI regimes described by the different statistical indicators.

|  | Linear stage | Nonlinear stage |
| --- | --- | --- |
| Complexity | Yes | Yes |
| $\kappa_4$ | No | Yes |
| SE | No | Yes |
| SSE | No | Yes |

exhibits a sharp decrease in the linear stage of MI well before $\kappa_4$ [Figs. 4(c) and 4(d)] and SE [Figs. 4(e) and 4(f)] start to vary appreciably. The sharp decrease in the computational complexity mirrors the self-organization process that shapes the random noise on top of the cw background into embryonic coherent structures. It is almost impossible to distinguish them from the cw background in the time domain [Figs. 2(f) and 2(g)] since the perturbations are several tens of decibels lower than the pump power [Figs. 2(b) and 2(c)]. However, in this linear MI regime apparently dominated by noise in the interval $P_{in} \in [0.3, 1.2]$ W, complexity varies substantially from 0.88 to 0.57. This illustrates the huge sensitivity of complexity to detect the early birth of coherent structures. Comparing with Fig. 3, we can appreciate how the value of $P_{in}$ at which coherent structure became visibly manifest is close to the value of $P_{in}$ around which computational complexity has its lowest value. After reaching a minimum for $P_{in} \approx 1.8$ W in experiment, computational complexity performs a series of damped oscillations. These oscillations occur in correspondence to the statistical signature of FPUT recurrences. The low value of computational complexity in the nonlinear stage of MI is indicative of the existence of coherent structures in the temporal

traces. Hence, on the one hand, computational complexity is a precursor of MI, and at the same time it characterizes the nonlinear stage dynamics. Computational complexity oscillations are analogous to the oscillations of $\kappa_4$ with the difference that maxima and minima are inverted in the two cases and that those of $\kappa_4$ are more pronounced. The connection between $\kappa_4$ and the statistical signature of FPUT recurrences has been already clearly demonstrated in Ref. [14]. SE exhibits oscillations in correspondence to FPUT recurrences too, but no appreciable variation in the linear stage of MI. The oscillations of SSE [Figs. 4(g) and 4(h)] are directly associated with the statistical signature of FPUT recurrences too and are aligned with the oscillations of the time domain statistical indicators. It is also worth stressing that simulations both with a cw input and with a pulsed input provide very similar results for all the indicators, the main difference being that SSE exhibits a small plateau at low power for the pulsed case (as in experiment), while this is not the case for the cw pumping. The small variation in SSE in the linear stage of MI is connected to the particular pulsed initial condition and is not directly connected to the MI process. In Table I a summary is presented of the different MI stages whose key features are captured or not by the various statistical methods investigated in this Research Letter. Computational complexity describes qualitatively both the growth of coherent structures from noise in the linear stage and the statistical signature of the recurrences in the nonlinear stage, while other methods despite fully capturing the nonlinear stage dynamics do not anticipate the growth of coherent structures in the linear stage. We observe some discrepancies affecting the quantitative, but not the qualitative, agreement between experimental and numerical results. In particular, we notice a sharper decrease of computational complexity and a lower average asymptotic value in numerical simulations compared with experiment. We believe that the main cause of these discrepancies is connected to the noise added to the signal after passing through the time lens before the detection, for which we do not have an appropriate model. We furthermore observed that the period of oscillations is slightly larger in experiments than in numerical simulations; this fact has been already noticed in Ref. [14] relative to the $\kappa_4$ indicator. In conclusion, we have provided a characterization of the computational complexity of MI of the NLSE homogeneous solution, using temporal trace data from a nonlinear fiber optics experiment. We have shown that computational complexity is a precursor which anticipates the formation of coherent structures initially embedded in noise, before they reach a distinguishable size and before the autocorrelation of the time traces and other well-known and used statistical indicators reveal appreciable variations. We have

furthermore shown that computational complexity correlates with the phenomenon of the statistical signature of FPUT recurrences consistently with other established statistical indicators. We anticipate that computational complexity could be used to provide relevant information about different MI and complex systems' behavior, both in photonics, for instance, to characterize the buildup process of pulses in mode-locked lasers and the nonlinear dynamics in optical resonators, and in other disciplines too, shedding light not only on the interplay between coherent structures and noise but also on statistical properties of asymptotic states.

[1] T. B. Benjamin, Instability of periodic wavetrains in nonlinear dispersive systems, Proc. Math. Phys. Eng. Sci. **299**, 59 (1967).

[2] T. Taniuti and Washimi, Self-Trapping and Instability of Hydromagnetic Waves Along the Magnetic Field in a Cold Plasma, Phys. Rev. Lett. **21**, 209 (1968).

[3] M. J. Ablowitz, *Nonlinear Dispersive Waves* (Cambridge University Press, Cambridge, 2011).

[4] V. Zakharov and L. Ostrovsky, Modulation instability: The beginning, Phys. D (Amsterdam) **238**, 540 (2009).

[5] K. Tai, A. Hasegawa, and A. Tomita, Observation of Modulational Instability in Optical Fibers, Phys. Rev. Lett. **56**, 135 (1986).

[6] P. Suret, R. El Koussaifi, A. Tikan, C. Evain, S. Randoux, C. Szwaj, and S. Bielawski, Single-shot observation of optical rogue waves in integrable turbulence using time microscopy, Nat. Commun. **7**, 13136 (2016).

[7] A. Tikan, S. Bielawski, C. Szwaj, S. Randoux, and P. Suret, Single-shot measurement of phase and amplitude by using a heterodyne time-lens system and ultrafast digital time-holography, Nat. Photonics **12**, 228 (2018).

[8] M. Närhi, B. Wetzel, C. Billet, S. Toenger, T. Sylvestre, J.-M. Merolla, R. Morandotti, F. Dias, G. Genty, and J. M. Dudley, Real-time measurements of spontaneous breathers and rogue wave events in optical fibre modulation instability, Nat. Commun. **7**, 13675 (2016).

[9] G. Van Simaeys, P. Emplit, and M. Haelterman, Experimental Demonstration of the Fermi-Pasta-Ulam Recurrence in a Modulationally Unstable Optical Wave, Phys. Rev. Lett. **87**, 033902 (2001).

[10] A. Mussot, C. Naveau, M. Conforti, A. Kudlinski, F. Copie, P. Szriftgiser, and S. Trillo, Fibre multi-wave mixing combs reveal the broken symmetry of Fermi-Pasta-Ulam recurrence, Nat. Photonics **12**, 303 (2018).

[11] D. Pierangeli, M. Flammini, L. Zhang, G. Marcucci, A. J. Agranat, P. G. Grinevich, P. M. Santini, C. Conti, and E. Del Re, Observation of Fermi-Pasta-Ulam-Tsingou Recurrence and Its Exact Dynamics, Phys. Rev. X **8**, 041017 (2018).

[12] G. Vanderhaegen, C. Naveau, P. Szriftgiser, A. Kudlinski, M. Conforti, A. Mussot, M. Onorato, S. Trillo, A. Chabchoub, and N. Akhmediev, "Extraordinary" modulation instability in optics and hydrodynamics, Proc. Natl. Acad. Sci. USA **118**, e2019348118 (2021).

[13] D. Solli, G. Henrik, and C. Ropers, Fluctuations and correlations in modulation instability, Nat. Photonics **6**, 463 (2012).

[14] A. E. Kraych, D. Agafontsev, S. Randoux, and P. Suret, Statistical Properties of the Nonlinear Stage of Modulation Instability in Fiber Optics, Phys. Rev. Lett. **123**, 093902 (2019).

[15] D. S. Agafontsev and V. E. Zakharov, Integrable turbulence and formation of rogue waves, Nonlinearity **28**, 2791 (2015).

[16] S. Toenger, T. Godin, C. Billet, F. Dias, M. Erkintalo, G. Genty, and J. M. Dudley, Emergent rogue wave structures and statistics in spontaneous modulation instability, Sci. Rep. **5**, 10380 (2015).

[17] A. Gelash, D. Agafontsev, V. Zakharov, G. El, S. Randoux, and P. Suret, Bound State Soliton Gas Dynamics Underlying the Spontaneous Modulational Instability, Phys. Rev. Lett. **123**, 234102 (2019).

[18] S. Wabnitz and B. Wetzel, Instability and noise-induced thermalization of Fermi-Pasta-Ulam recurrence in the nonlinear Schrödinger equation, Phys. Lett. A **378**, 2750 (2014).

[19] R. Badii and A. Politi, *Complexity* (Cambridge University Press, Cambridge, 1997).

[20] L. Leuzzi, C. Conti, V. Folli, L. Angelani, and G. Ruocco, Phase Diagram and Complexity of Mode-Locked Lasers: From Order to Disorder, Phys. Rev. Lett. **102**, 083901 (2009).

[21] C. Conti and L. Leuzzi, Complexity of waves in nonlinear disordered media, Phys. Rev. B **83**, 134204 (2011).

[22] N. Ghofraniha, I. Viola, F. Di Maria, G. Barbarella, G. Gigli, L. Leuzzi, and C. Conti, Experimental evidence of replica symmetry breaking in random lasers, Nat. Commun. **6**, 6058 (2015).

[23] D. Pierangeli, A. Tavani, F. Di Mei, A. J. Agranat, C. Conti, and E. DelRe, Observation of replica symmetry breaking in disordered nonlinear wave propagation, Nat. Commun. **8**, 1501 (2017).

[24] G. Parisi, Infinite Number of Order Parameters for Spin-Glasses, Phys. Rev. Lett. **43**, 1754 (1979).

[25] M. Mezard, G. Parisi, and M. Virasoro, *Spin Glass Theory and Beyond* (World Scientific, Singapore, 1986).

[26] F. Kaspar and H. G. Schuster, Easily calculable measure for the complexity of spatiotemporal patterns, Phys. Rev. A **36**, 842 (1987).

[27] A. N. Kolmogorov, On tables of random numbers, J. Statist., Ser. A **25**, 369 (1963) [Theor. Comput. Sci. **207**, 387 (1998)].

[28] A. Lempel and J. Ziv, On the complexity of finite sequences, IEEE Trans. Inf. Theory **22**, 75 (1976).

[29] C. E. Shannon, A mathematical theory of communication, Bell Syst. Tech. J. **27**, 379 (1948).

[30] C. Conti, M. Peccianti, and G. Assanto, Complex dynamics and configurational entropy of spatial optical solitons in nonlocal media, Opt. Lett. **31**, 2030 (2006).

[31] A. Petrosian, Kolmogorov complexity of finite sequences and recognition of different preictal EEG patterns, in *Proceedings of the Eighth IEEE Symposium on Computer-Based Medical Systems* (IEEE Computer Society, Los Alamitos, CA, 1995), pp. 212–217.

[32] D. Abásolo, R. Hornero, C. Gómez, M. García, and M. López, Analysis of EEG background activity in Alzheimer's disease patients with Lempel-Ziv complexity and central tendency measure, Med. Eng. Phys. **28**, 315 (2006).

[33] X. Zhang, Y. Zhu, and X. Zhang, New approach to studies on ecg dynamics: Extraction and analyses of QRS complex irregularity time series, Med. Biol. Eng. Comput. **35**, 467 (1997).

[34] J. M. Amigó, J. Szczepański, E. Wajnryb, and M. Sanchez-Vives, Estimating the entropy rate of spike trains via Lempel-Ziv complexity, Neural Comput. **16**, 717 (2004).

[35] V. D.Gusev, L. A.Nemytikova, and N. A.Chuzhanova, On the complexity measures of genetic sequences, Bioinformatics **15**, 994 (1999).

[36] G. P. Agrawal, *Nonlinear Fiber Optics*, 5th ed. (Academic, San Diego, CA, 2012).

[37] R. Salem, M. A. Foster, and A. L. Gaeta, Application of space-time duality to ultrahigh-speed optical signal processing, Adv. Opt. Photonics **5**, 274 (2013).